Graph-Based Modeling and Molecular Dynamics for Ion Activity Coefficient Prediction in Polymeric Ion-Exchange Membranes

P. Naghshnejad,[a,τ] G. Theis Marchan,[a,τ] T. Olayiwola,[a] R. Kumar,[b] J. A. Romagnoli[a,*]

[a] Department of Chemical Engineering, Louisiana State University, Baton Rouge, LA 70803
[b] Department of Chemistry, Louisiana State University, Baton Rouge, LA 70803

[τ] These two authors contributed equally to this study.

* Contact information : Professor Jose A. Romagnoli, jose@lsu.edu

ABSTRACT

The partitioning of ions between polymeric ion-exchange membranes (IEMs) and the surrounding liquid is governed by the activity coefficients of the ions, which, in turn, significantly impact various ion transport processes within these membranes, notably conductivity. This study introduces a computational framework to predict ions' activity coefficients in charged Ion Exchange Membranes (IEMs). This method employs a machine learning (ML) model using molecular-scale characteristics obtained from Molecular Dynamics (MD) simulations, particularly emphasizing solvation properties within the context of IEMs. Specifically, the framework utilizes Graph Convolutional Networks (GCN) to establish connections between the chemical structure of the polymer and the molecular-level attributes. This ultimately leads to determining macroscopic attributes, such as the activity coefficient, across a range of IEM materials, having random copolymer and block copolymer systems. Furthermore, saliency maps were generated to identify the critical features of polymer molecules that correlate with ion activity coefficients. The graph-based prediction strategy proved highly accurate in predicting ion activity coefficients within IEMs, even with relatively small training datasets.

1. INTRODUCTION

Ionic separations have a great impact in water desalination and ultra-pure water production for semiconductors, food, and pharmaceutical applications.[1] Furthermore, they are increasingly recognized as valuable tools for recovering organic acids from processed biomass streams[2, 3] and extracting valuable metals from waste and hydrometallurgy streams,[4] in addition to addressing the remediation of water contaminated with undesirable substances (e.g., perfluoroalkyl and poly-fluoroalkyl substances (PFAS)[5, 6] and heavy metals[7, 8]). These electrically driven ionic separations encompass relying on ion-exchange membranes (IEMs).

The chemical structure of these IEMs significantly affects their ionic conductivity, perm selectivity, and other transport properties, such as osmotic drag.[9-12] Consequently, the molecular structure of IEMs profoundly influences these properties. As a result, polymeric IEMs involve several parameters affecting conductivity and perm selectivity. In chemistry, activity coefficients hold pivotal significance as they provide insights into the behavior of solutions, particularly deviations from non-ideal behavior.[13] These coefficients are essential for comprehending phase equilibria,[14, 15] solubility,[14, 16] and chemical reactions,[16] making them indispensable for a broad spectrum of industrial and scientific applications. The ion activity coefficients within polymeric IEMs govern the balance of ion distribution between the membrane and the surrounding liquid. Furthermore, these coefficients directly impact electrical conductivity within ion-exchange membranes.

Historically, the prediction of activity coefficients often relied on intricate mathematical models and extensive experimental data. Using Computational models that can relate molecular descriptors to material properties are very important for developing and optimizing these systems.[17] Therefore, molecular dynamics (MD) is a versatile and valuable tool for understanding the solvation process and the arrangement of counterions and ionic groups along the polymer backbone.[1] This information is instrumental in elucidating the observed conductivity and ionic activity in experimental settings for IEMs. However, this analytical method involves the simulation of large system sizes and requires considerable time, which can pose a significant challenge because of the high computational cost. Thus, developing strategies to alleviate the computational cost issue is essential. Over the past decade, machine learning (ML) techniques have been used as data-driven technics that help molecule screening and decrease experimentation

costs, especially when a large system is involved.[18] Moreover, Graph Neural Networks (GNNs)[19, 20] have been under special attention in the field of chemistry, offering an innovative approach to modeling and predicting diverse molecular properties in various applications such as chemical engineering,[21] (quantum) chemistry[19, 22, 23] and the prediction of physical[24, 25] and crystal properties.[26] GNNs present a data-driven and machine learning-centric strategy that captures intricate relationships within molecular structures to yield more precise forecasts. This marks a significant advancement in our ability to comprehend and predict the behavior of complex molecular properties. For instance, Wu et al.[27] used graph neural networks (GNNs) trained on molecular graphs to predict variety of molecular properties. Qin et al.[28] designed a simple graph convolutional network (GCN) architecture to predict critical micelle concentrations (CMCs) of surfactants directly from their molecular representation. Kensert et al.[29] implemented GCN to predict the retention times of molecules for three chromatographic datasets. However, most studies in this area have been on the prediction of different molecular properties characterized by a considerable volume of datasets.

Despite these advancements, the application of Graph Neural Networks (GNNs) for predicting activity coefficients within charged Ion Exchange Membranes (IEMs) remains an unexplored territory. This work addresses this gap by introducing a groundbreaking computational framework that seamlessly integrates machine learning (ML) methods with molecular dynamics (MD) simulations. Specifically, our approach leverages Graph Convolutional Networks (GCN), a fundamental architecture in the family of GNNs, to predict the activity coefficients of ions within IEMs. The model harnesses molecular-scale descriptors derived from MD simulations, focusing on solvation properties within the unique context of IEMs. By establishing connections between the chemical structure of the polymer and molecular-level attributes, the framework determines macroscopic attributes, such as the activity coefficient of IEMs. This novel method not only breaks new ground in efficiently predicting and understanding the behavior of ions in electrochemical separation platforms but also demonstrates the transformative potential of integrating ML and MD techniques for advancing the field of ion behavior prediction in polymeric membranes. Moreover, experimental data related to ion activity coefficients in polymeric IEMs were collected for training and validation purposes. These data encompassed information concerning the structure of polymer, ion exchange capacity, water uptake, and ion activity coefficients[1]. Furthermore, saliency maps were generated to identify key features of polymer molecules that correlate with ion activity

coefficients. Impressively, the ML-MD modeling strategy yielded highly accurate predictions of ion activity coefficients within IEMs, with an error rate of less than 7%. Remarkably, this predictive accuracy was achieved with small training datasets.

2. METHODOLOGY

2.1. GCN Architecture

The visual representation provided in **Figure 1** depicts the two innovative architectures proposed for the precise prediction of activity coefficients in Ion exchange membranes. Each stage of the architecture has been meticulously designed to contribute to the exceptional performance of the model. Both architectures begin with different data structures, such as polymer structure, and salt structure (**Figure 1a and b**). These are input to a graph convolutional neural network (GCN) consisting of two convolutional layers and the ReLU activation function. These layers are designed to encode the molecular features into a format suitable for further analysis.

In the second architecture (**Figure 1b)**, additional features inputs derived from MD simulations are incorporated to enhance the predicted performance. These inputs consist of twelve (12) parameters known as MD descriptors[1], such as coordination numbers from the first solvation shell and different radial distribution functions (RDF). RDF descriptors in our dataset notably encompass the positions of first minima and peak heights, as well as peak positions and coordination numbers associated with the counterion and the oxygen of water molecules, tethered charge, and counterions. Then, concatenated the transformed graph-based molecular representations with critical features such as salt concentration, water per ion and the MD descriptors, forming a comprehensive feature vector that encapsulates both the graph-derived and scalar properties.

The final stage of the architecture is a feedforward neural network (FNN) that utilizes the combined feature set. This FNN is intricately designed with three linear hidden layers, each contributing to the refinement of the data towards the ultimate goal: predicting activity coefficients with high precision. The FNN serves as the decisive predictive component of the architecture, outputting activity coefficients that reflect the non-ideal behavior of species in the IEM systems. The model was constructed using PyTorch[30] (version 2.2).

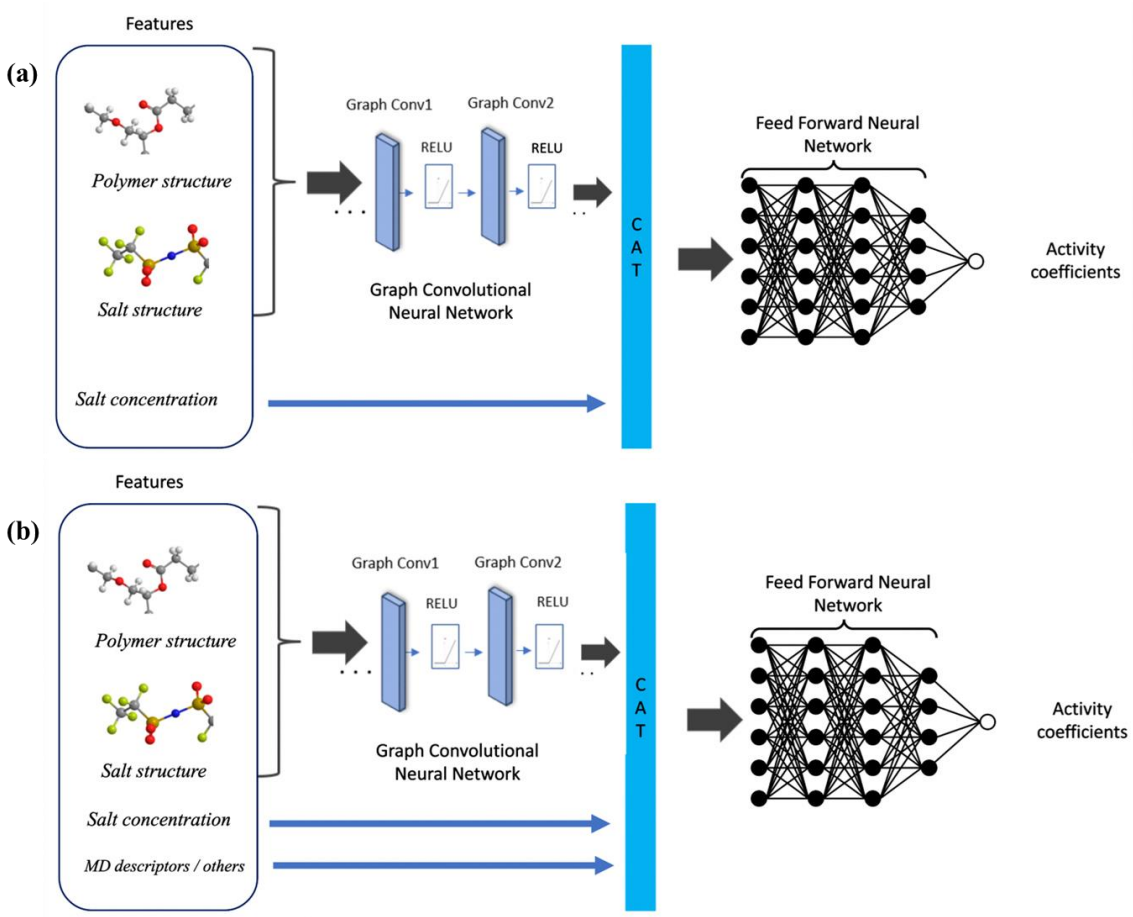

Figure 1: Methodology architecture workflow (a)without molecular dynamics descriptors and others and (b) with molecular dynamics descriptors and others.

2.2. Predictive Model (GCN)

GCN is a type of CNN specifically modeled based on graph data, utilizing the inherent graph structure to process non-Euclidean structured data, such as molecular structures.[31-33] The input to a GCN is typically a SMILES string representing a molecule changed into a molecular graph $\mathcal{G} = \{\mathcal{V}, \mathcal{E}\}$ using RDKit.[34] **Figure 2** illustrates this transformation process, where nodes ($\mathcal{V}$) represent atoms, and edges ($\mathcal{E}$) denote the bonds between these atoms. Prior to graph encoding, it is crucial to define and specifies the node features within a feature matrix (X). These features, including the atomic type, atomic element, the number of additional hydrogen atoms, the number of valences, and aromaticity, are encoded using a one-hot encoding strategy. **Table 1** details the atom features

utilized in constructing the feature matrix. Essentially, GCN learn the representation of each atom by getting the information from its neighboring atoms encoded by the node feature matrix and the information of the connected bonds encoded by the adjacency matrix ($\tilde{A}$) through message passing across the molecular graph recursively passed by the state updating of the central atoms and read-out operation.[35, 36]

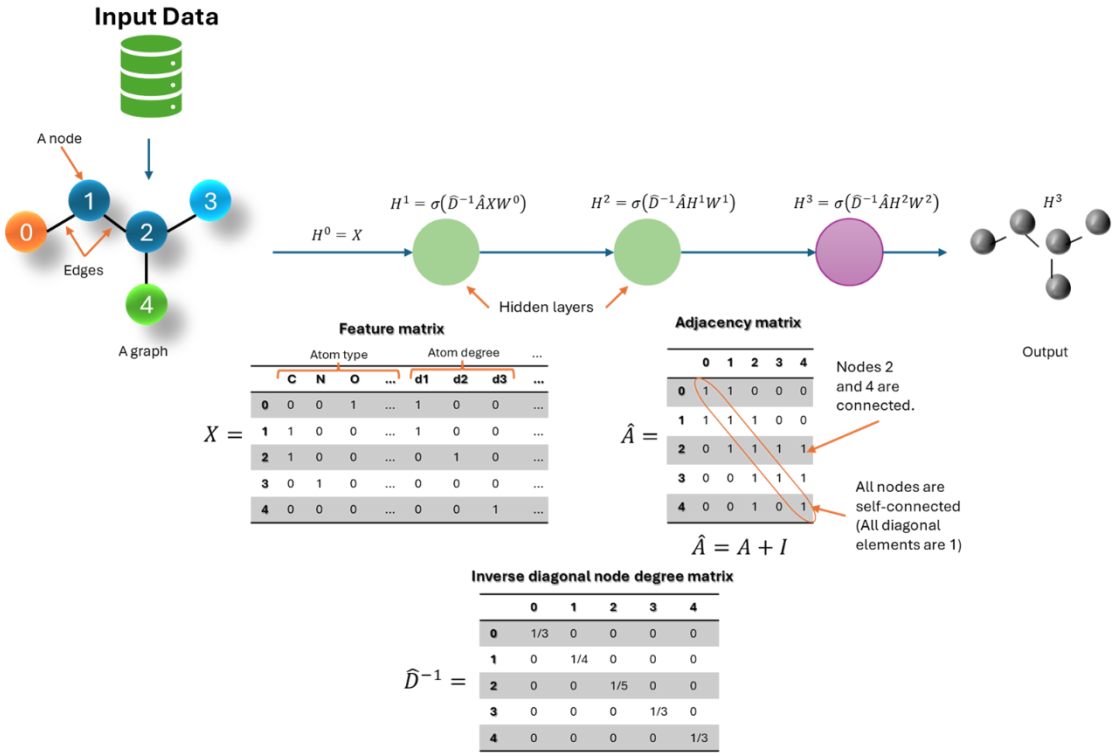

Figure 2: Simplistic representation in graph convolutional neural network architecture. Atoms are shown as nodes and bonds represented as edges. The feature matrix encoded the neighboring atoms, and the adjacency matrix indicates the neighbors of a node and designates that all nodes are self-connected. Since, GCN wants $\tilde{A}$ to be normalized to maintain the scale of the output feature vector, $\tilde{D}^{-1}$ is introduced, where $\tilde{D}$ is the diagonal node degree matrix of $\tilde{A}$ in measuring the degree of each node. The equation of propagation rule ($H^{i+1} = \sigma(\hat{D}^{-1}\hat{A}H^iW^i)$) is used to compute a hidden layer output from the last layer output. It is based on the classical GCN model proposed in 2016.[37]

The underlying mathematics aligns with the classical GCN model proposed by Kipf et al.[37] (2016), which employs a layer-wise propagation rule shown in equations (1) and (2).

$$H^{(l+1)} = f(H^{(l)}, A) \quad (1)$$

$$H^{(l+1)} = \sigma(\tilde{D}^{-\frac{1}{2}}\tilde{A}\tilde{D}^{-\frac{1}{2}}H^{(l)}W^{(l)}) \quad (2)$$

where $H^{(l)}$ and $W^{(l)}$ represent the l-th layer of the neural network and its parameters, respectively, with $H^{(0)} = X$. The non-linear activation function, denoted by σ is often the $ReLU(\cdot) = \max(0,\cdot)$ function. D and A correspond to the degree and adjacency matrices, respectively, with $\tilde{A} = A + I$ (I is the identity matrix), and $\tilde{D}$ being the diagonal node degree matrix of $\tilde{A}$ and $\tilde{D}^{-1}$ the inverse of $\tilde{D}$. The construction of the term $\tilde{D}^{-\frac{1}{2}}\tilde{A}\tilde{D}^{-\frac{1}{2}}$ aims to introduce a self-connection for each node and maintain the scale of the feature vectors. In the context of activity coefficients, this approach facilitates the accurate estimation of solute-solvent interactions, structural dependencies, and phase behavior.

Table 1: List of atom features.

Atom Feature	Size	Description
Atom type	43	[B, C, N, O, F, Si, P, S, Cl, As, Se, Br, Te, I, At, metal] (one-hot)
Atom degree	44-54	Number of connected bonds (one-hot)
Hydrogens	55-61	Number of implicit Hs (one-hot)
Formal charge	62	Electrical charge (integer)
Radical electron	63	Number of radical electrons (integer)
Hybridization	64-68	(sp, sp2, sp3, sp3d, sp3d2) (on-hot)
Aromaticity	69	Whether the atom is part of the aromatic system (one-hot)

2.3. Molecular Dynamics Simulations

Canonical MD simulations were done to get molecular information of activity coefficient. These simulations can calculate the solvation descriptors of IEMs at the atomic level. In previous studies conducted by our group,[38, 39] it was shown that the molecular solvation environment, including hydration and ion pairing, around the ionic species determined from the associated radial distribution functions (RDFs) as well as water cluster size probability distributions from MD simulations corresponds to the extent of counterion condensation and ion dehydration as well as ion activity coefficients and conductivity from experiments of polyelectrolytes in aqueous media. Hence, given this strong correlation of molecular level characteristics on polyelectrolyte properties, in this study, we employed MD simulations to determine the solvation descriptors

obtained from the relevant ion radial distribution functions. As depicted in **Figure 3**, our simulation workflow initiates with the input of polymer IEMs and salt ions, proceeding through the MD simulations, and ends with the derivation of the solvation descriptors. The radial distribution function $g(r)$ is fundamental to our analysis, offering insights into the ion pairing and the degree of association between charged species.

The activity coefficients inferred from the $g(r)$ characteristics are indicative of the intricate behaviors and properties of the IEMs, which are influenced by variables such as polymer structure, salt type, and concentration. These coefficients provide a gateway for machine learning models to predict ion behavior in electrochemical separation processes, effectively linking molecular dynamics findings to macroscopic properties.

The methodology utilized in molecular dynamics (MD) simulations for the study of ion exchange polymeric IEMs involves a comprehensive and detailed computational approach. By harnessing the increased computational power available, our group[1] conducted approximately 100 classical canonical MD simulations using the LAMMPS[40] software to analyze the activity coefficients of ions within these systems. The MD simulations were done on a cubic system of around 40 Å, including IEMs, ions, and water molecules. The design of IEMs is done by either the OPLS-AA[41, 42] or GAFF2[43] force fields, while water molecules were represented by the TIP3P[44] force field. Computational chemistry tools such as GAUSSIAN[45] and ANTECHAMBER determined the partial charges of the constitute elements of Ion exchange membranes,[46] depending on the chosen force field.

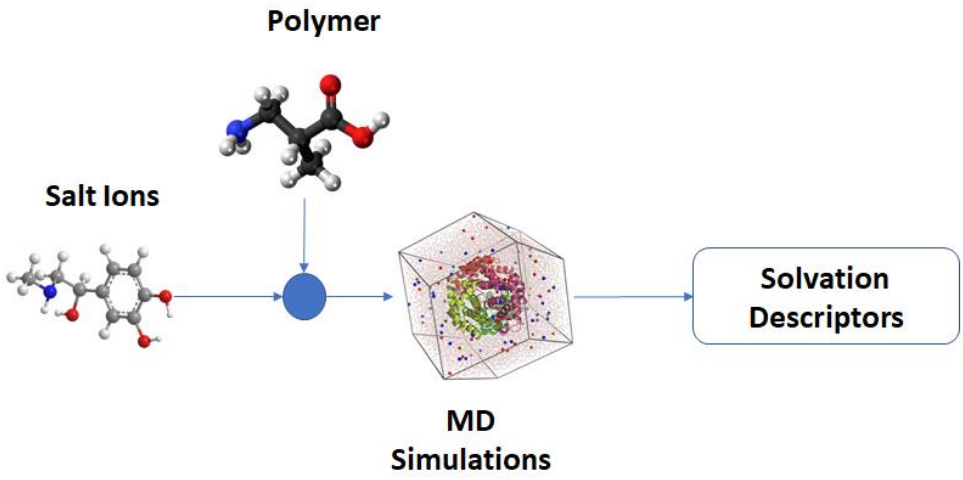

Figure 3: Workflow of the molecular dynamic simulation.

2.4 Understanding Features: Saliency Maps

Saliency maps serve as a visualization technique designed to elucidate the specific areas within an input sample that significantly influences the output decision generated by a classification system.[47] They can be regarded as a form of sensitivity analysis widely applicable across various research domains.[28, 47-49]

A saliency map aligns with the input dimensions and encapsulates the importance values attributed to each component, thereby delineating their individual contributions to the output. The calculation method applied involves backpropagation-based approaches, which implies obtaining the important information from the gradient of the output with respect to the input. The gradient explanation for an input x is $E_{grad}(x) = \frac{\partial S}{\partial x}$. In our formal setup, the input x represents the atom feature vectors and S represents the predicted activity coefficients. In that sense, the gradient quantifies how much an alteration in each input dimension would change the predictions $S(x)$ in a small neighborhood around the input.[50] A second approach would multiply the gradient by the input values, denoted as $x \odot \frac{\partial S}{\partial x}$, to leverage out the gradients that do not carry relevant information.[50]

To determine the influence of specific atom types on the predictions of activity coefficients at a node level, we aggregated the gradients associated with atom types as shown in equation (3). We then normalized these aggregated gradient values to fall within a range of −1 to 1, ensuring

the original sign of each gradient value was preserved during the normalization process. The gradient calculation and visualization of the saliency was constructed using chainer-chemistry[51].

$$Saliency = \sum_{x \in atom\ type} x \odot \frac{\partial S}{\partial x} \quad (3)$$

3. DATA AND HYPERPARAMETER

3.1. Datasets and Model Training

The utilized dataset comprises a comprehensive combination of experimental and molecular dynamics (MD) data, which served as the foundational elements of the study conducted in our group by Gallage Dona et. al.[1] The experimental data comprises 12 copolymer IEMs, with thin films interfaced with different salt concentrations (0.02, 0.2, 0.5), and the number of water molecules per tethered ions along with their respective ion activity coefficients. The data compiled in this study contains ionomers with varying arrangements of monomeric units, such as random-termed random copolymer electrolyte (RCE) and block-termed block copolymer electrolyte (BCE). Additionally, the ionomers have different numbers of side chains and counterions for the charged monomers. Someof these copolymers are AR103,[13] AR204,[13] CR61,[13, 52] Nafion,[53] polyvinyl alcohol sulfate PVAS,[13, 54] poly(styrene-block-2-vinylpyridine/n-methylpyridinium iodide) PSbNMP,[38, 39] poly(2-acrylamido-2-methylpropanesulfonic acid-block-diethylene glycol dimethacrylate) CEM,[55] poly(ethylene glycol)diacrylate, and 2-acrylamido-2-methyl-1-propanesulfonic acid (XL-AMPSPEGDA).[56] It is important to note that AR103, AR204, Nafion, and CR61 are commercial IEMs. For the conversion of polymers and salts into SMILES representations, RDKit[34] package was used (Polymer structure can be found in Table S2).

However, the molecular dynamics data consists of twelve (12) solvation descriptors calculated from molecular dynamics simulations as input variables. **Table 2** describes the 12 solvation descriptors and the experimental parameters considered in this study. Therefore, the total data set contains 80 points for the prediction of activity coefficients. (Table S1)

The data set was split into training (~80%) and testing (~20%) subsets and performing K-fold cross-validation (CV) shown in **Figure 4** for hyperparameter tuning. In the *k*-fold Cross-validation, the training subsets were randomly divided into *k* groups. The model was then trained *k* times with

different groups held out each time as the validation set and the remaining *k*-1 groups used as training set.

Table 2: Description of the dataset parameters.[1]

Dataset parameters	Type of data
Polymer name	Experimental data
Salt	Experimental data
Number of water molecules per tethered ions	Experimental data
Concentration of salt	Experimental data
first minima of RDF between the counterion and oxygen of water.	MD Solvation descriptor
peak position of RDF between counterion and oxygen of water	MD Solvation descriptor
peak height of RDF between counterion and oxygen of water	MD Solvation descriptor
coordination number (at first minima) from RDF between counterion and oxygen of water	MD Solvation descriptor
first minima of RDF between tethered charge (in IEMs) and oxygen of water	MD Solvation descriptor
peak position of RDF between tethered charge (in IEMs) and oxygen of water	MD Solvation descriptor
peak height of RDF between tethered charge (in IEMs) and oxygen of water	MD Solvation descriptor
coordination number (at first minima) from RDF between tethered charge (in IEMs) and oxygen (in water)	MD Solvation descriptor
first minima of RDF between tethered charge (in IEMs) and counterion (in salt)	MD Solvation descriptor
peak position of RDF between tethered charge (in IEMs) and counterion (in salt)	MD Solvation descriptor
peak height of RDF between tethered charge (in ionomer) and counterion (in salt)	MD Solvation descriptor
coordination number (at first minima) from RDF between tethered charge (in ionomer) and counterion (in salt)	MD Solvation descriptor
ion activity coefficients in IEMs	Experimental data

3.2. Hyperparameters optimization and cross-validation.

We experimented with several key hyperparameters, including the number of hidden neurons (either 128 or 256), and the learning rate (0.01, 0.005, or 0.001, and 0.0005), and a batch size of 10 and 20 and different random seed numbers as shown in Error! Reference source not found.. The model was trained with a mean-squared-error loss function, using the Adam optimizer. The maximum epoch was set to 1000, and when early stopping was enabled, the training process was terminated, to prevent the issues of overfitting. K-fold Cross-validation was also conducted to prevent overfitting. This method involves partitioning the dataset into k subsets, where each subset serves as a validation set in turn while the remaining k-1 subsets are used for training. This process iterates k times, with each subset being used exactly once as the validation set (**Figure 4:** schematic of the process of hyperparameter optimization through k-fold cross-validation for training, testing, and). Through this iterative process, hyperparameters are optimized to ensure robustness and generalization of

the model across diverse datasets. The performance of the model is quantified by four metrics such as mean-square error (RMSE), mean absolute error (MAE), the determination coefficient R^2 and the standard deviation, which can respectively measure the accuracy and the proportion of the variation of predicted results (Error! Reference source not found.).

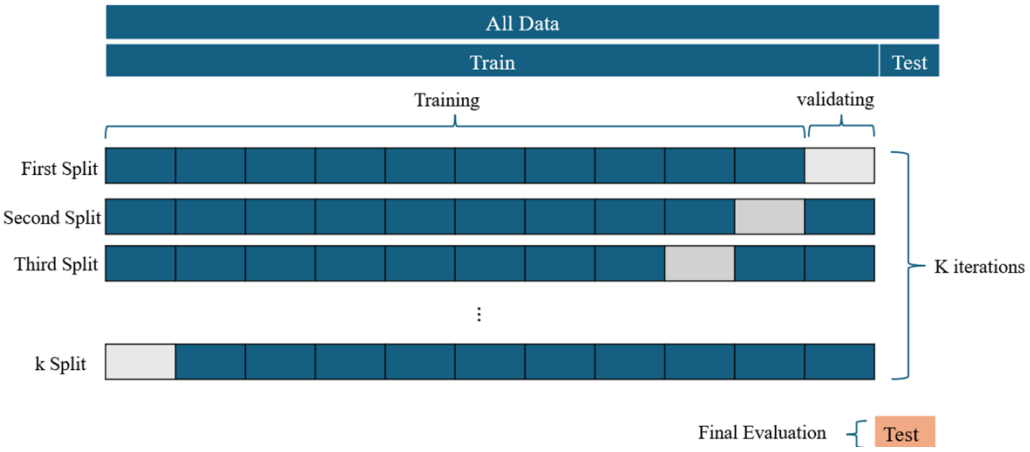

Figure 4: schematic of the process of hyperparameter optimization through k-fold cross-validation for training, testing, and validation.

4. RESULTS AND DISCUSSION

4.1. Hyperparameter Tuning

Analysis of graph convolutional models (GCNs) with and without the integration of molecular dynamics (MD) descriptors, considering various hyperparameters was done in **Table 3**. Through systematic experimentation, the performance of GCNs in prediction of activity coefficient was evaluated based on different seed numbers, batch sizes, hidden layer configurations, and learning rates. Our findings elucidate the impact of MD integration on model performance and provide insights into optimal hyperparameter configurations for accurate property prediction.

Models incorporating MD descriptors consistently demonstrate higher R^2 scores and lower MAEs compared to those without MD descriptors across various hyperparameter configurations (**Table 3**), indicating the beneficial impact of integrating dynamic molecular information on predictive accuracy and generalization capability. While GCN architectures are known to be sensitive to hyperparameter settings, models with MD integration exhibit better robustness to

hyperparameter variations, as evidenced by their more consistent performance across different experimental setups. Certain hyperparameter configurations lead to superior performance for GCN architectures. For example, configurations featuring moderate batch sizes, deeper hidden layers, and optimal learning rates tend to yield higher R^2 values and lower MAEs, thus indicating enhanced predictive accuracy and generalization capability. The accompanying figure clearly illustrates the influence of incorporating MD simulation descriptors on the performance of GCN models. Within the scope of our analysis, a GCN model equipped with MD descriptors achieved the maximum R^2 at a learning rate (LR) of 0.0005 and 128 hidden neurons (HN), suggesting an optimal balance between learning efficiency and the network's ability to model the complexity of the data. Interestingly, increasing the number of hidden neurons to 256 did not significantly decrease the R^2, indicating a certain robustness of the model to capacity expansion within the tested range. Conversely, models lacking MD descriptors exhibited greater sensitivity to variations in hyperparameters, hinting at potential instability in the learning process, likely due to the absence of stabilizing information typically provided by MD descriptors. Another indication of the robustness of the Graph Convolutional Network (GCN) model integrated with Molecular Dynamics (MD) lies in its consistent performance across various random seed numbers used during training. In contrast, the model lacking MD descriptors exhibits significant variability in performance when different seed numbers are employed. For instance, with seed number 28 and a batch size of 10, both the coefficient of determination (R^2) for training and testing data remains at approximately 0.6, indicating a notably low fit compared to other seed numbers. However, the utilization of MD descriptors mitigates this variability, as evidenced by the stability of the model's performance across different seed numbers.

Table 3: performance of graph convolutional models (GCNs) without the integration of molecular dynamics (MD) Considering Different Hyperparameters.

seed	Batch size	hidden layer	learning rate	Without MD Descriptors				With MD Descriptors			
				R^2 (train)	R^2 (test)	MAE (train)	MAE (test)	R^2 (train)	R^2 (test)	MAE (train)	MAE (test)
28	10	256	0.005	0.653	0.625	0.118	0.103	0.987	0.984	0.026	0.037
28	20	256	0.005	0.958	0.964	0.059	0.053	0.965	0.936	0.05	0.06
48	10	256	0.005	0.971	0.656	0.056	0.109	0.989	0.859	0.030	0.055
48	20	256	0.005	0.985	0.722	0.036	0.092	0.988	0.859	0.03	0.054
42	20	256	0.005	0.967	0.937	0.049	0.066	0.983	0.961	0.032	0.050
42	10	256	0.005	0.966	0.922	0.047	0.067	0.967	0.96	0.044	0.057
42	10	256	0.01	0.976	0.928	0.043	0.079	0.976	0.928	0.043	0.079
42	10	256	0.001	0.960	0.932	0.046	0.065	0.981	0.971	0.033	0.049
42	10	256	0.0005	0.984	0.947	0.030	0.058	0.981	0.966	0.034	0.049
42	10	128	0.005	0.967	0.936	0.041	0.062	0.968	0.97	0.051	0.046
42	10	128	0.01	0.955	0.926	0.060	0.078	0.978	0.968	0.038	0.054
42	10	128	0.001	0.976	0.943	0.036	0.060	0.989	0.951	0.026	0.055
42	10	128	0.0005	0.986	0.959	0.028	0.057	0.983	0.975	0.032	0.045

Figure 5 illustrate the consistent superiority of GCN models enhanced with MD descriptors over those without, across various hyperparameter configurations. The data presented in these figures is based on random seed number 42, with variations in hidden neurons and learning rate. Specifically, models incorporating descriptors yielded higher R^2 values, indicating superior predictive capability (**Figure 5**). This improvement underscores the critical role of MD descriptors in capturing the intricate dynamics of the dataset, thereby enhancing model accuracy. The x-axis represents different hyperparameter combinations, including learning rate (LR) and number of hidden layers (HN), with each bar corresponding to a specific LR-HN combination. The y-axis represents R^2 values, measuring the goodness of fit of GCN models, with higher values indicating better fit.

The figure clearly illustrates the impact of integrating MD simulation descriptors on GCN model performance. Notably, increasing hidden neurons to 256 did not significantly reduce R^2, suggesting the model's robustness within the tested range. Conversely, models lacking MD descriptors exhibited greater sensitivity to hyperparameter variations, possibly indicating instability in the learning process due to the absence of stabilizing MD information.

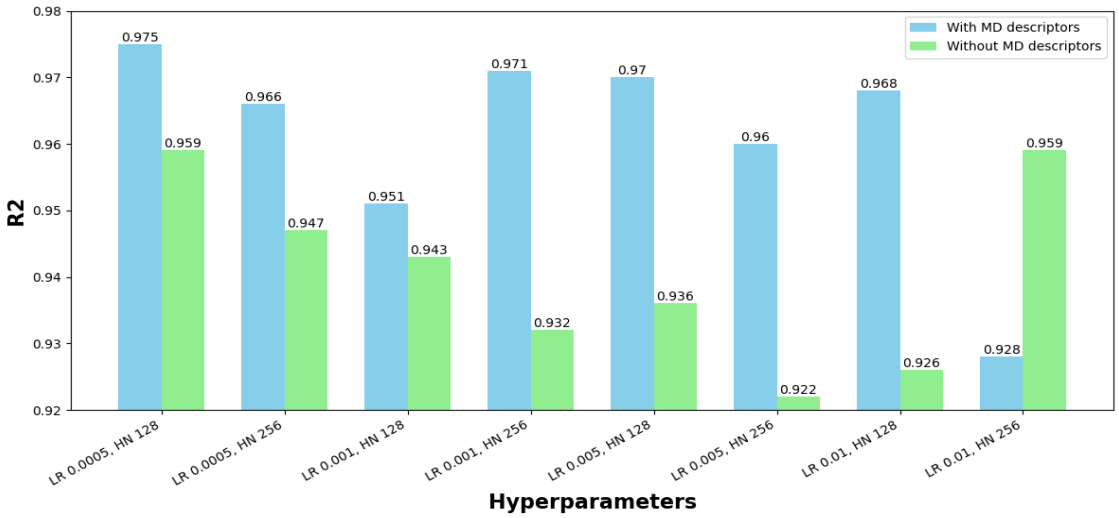

Figure 5: Performance comparison based on R^2 value of graph convolutional networks (GCNs) with and without molecular dynamics (MD) simulation descriptors.

The investigation of Mean Absolute Error (MAE) in **Figure *6*** revealed a nuanced trade-off between the minimization of average prediction errors and the maximization of variance explained. The x-axis represents different hyperparameter combinations, specifically the learning rate (LR) and the number of hidden layers (HN). Each bar corresponds to a specific combination of LR and HN. The y-axis denotes the MAE values, which quantify the average deviation between predicted and actual values. Lower MAE values show better performance and higher accuracy of the GCN models. The figure provides insights into the impact of including MD simulation descriptors on the performance of GCN models in predicting molecular properties. Across various hyperparameter combinations, the MAE values tend to be consistently lower when MD descriptors are utilized, as indicated by the navy-blue bars. This suggests that the inclusion of MD descriptors leads to improved accuracy and reduced error in the predictions made by GCN models compared to those trained solely on non-MD descriptors. The most favorable MAE was recorded at an LR of 0.0005 with 128 HN for models equipped with MD descriptors, the same hyperparameter configuration that optimized R^2.

Overall, the figure highlights the importance of leveraging MD simulation data to enhance the predictive capabilities of GCN models for the task at hand, ultimately leading to more accurate predictions of molecular properties.

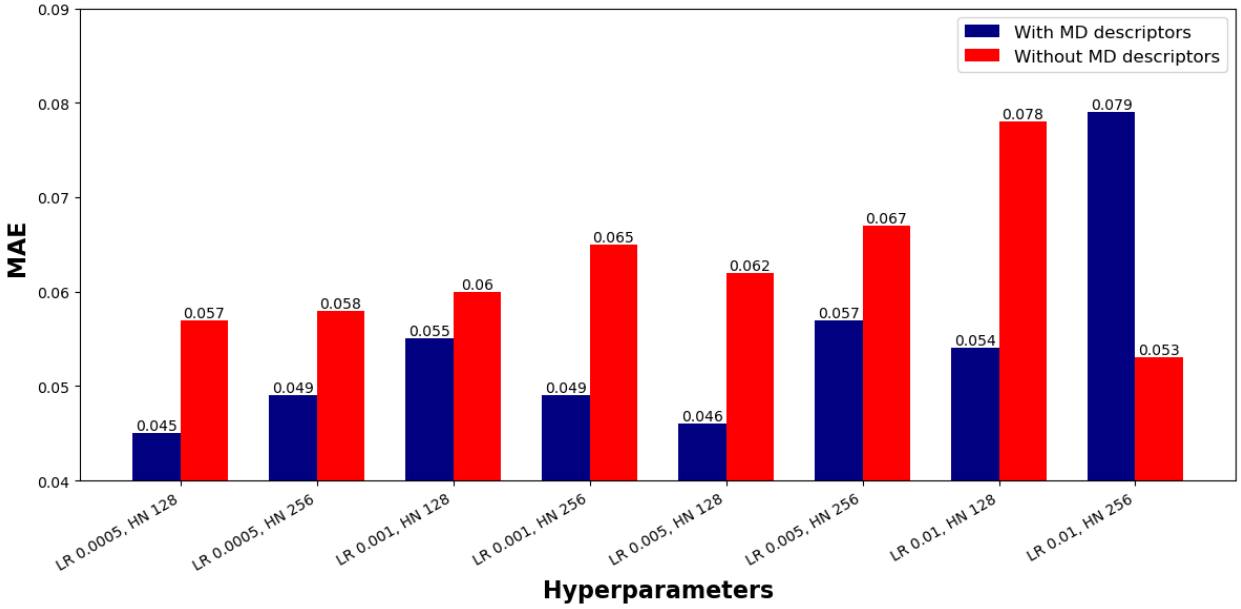

Figure 6: The comparison of mean absolute error (MAE) values obtained from graph convolutional networks (GCNs) with and without the incorporation of molecular dynamics (MD) simulation descriptors. Two sets of bars are presented in the figure.

4.2. Effect of MD Descriptor on Activity Coefficient Prediction

Figure 7 illustrates the parity plots comparing the predicted and experimental activity coefficients. These plots serve as a visual representation of the model's accuracy, with a closer clustering of data points around the line of unity indicating higher accuracy. In **Figure 7**, the incorporation of MD descriptors demonstrates a marked improvement in model performance (seed number 28 with a batch size of 10, 256 hidden neurons, and a learning rate of 0.005), as evidenced by the R^2 values of 0.987 and 0.984 for the train and test sets, respectively. In contrast, the model lacking MD descriptors (**Figure 7.b**) exhibits a notable decline in predictive accuracy, for the train and test set, where the R^2 value drops to 0.653 and 0.625, respectively. The divergence of both training and test accuracy performance of activity coefficient above 1. This underscores the importance of molecular dynamics (MD) descriptors, particularly in scenarios where there is interaction between polymer and salt, a concept consistent with the definition of molecular dynamics.

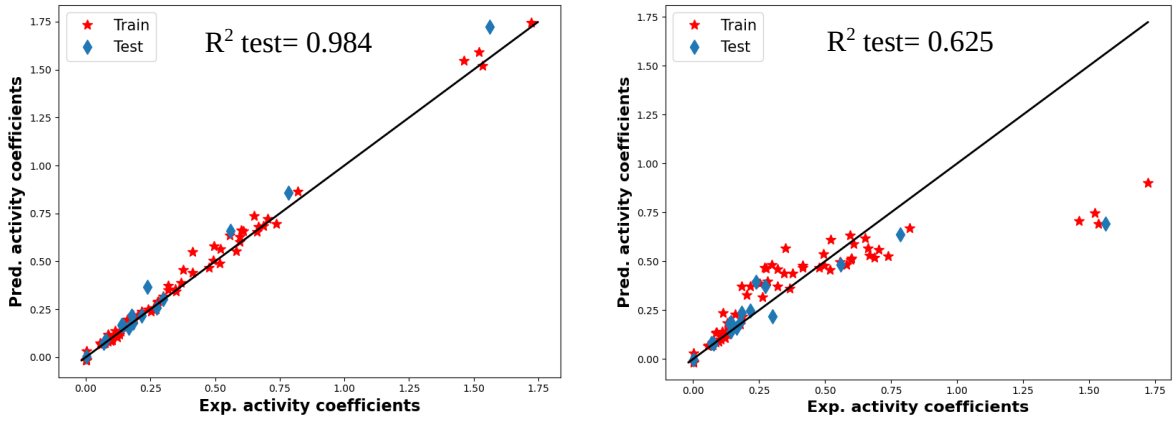

(a) (b)

Figure 7: Parity plot between predicted and experimental activity coefficient with MD descriptors and (b) without MD descriptors.

By looking closely at **Figure 7**, we see a big difference between with and without descriptors for polymers associated with high activity coefficient. The polymers associated with activity coefficient values above 1 in our dataset include XLAPn4_9p (shown in **Figure 8**). This prominence directs our focus towards understanding the molecular dynamics effect on activity coefficient value. A meticulous analysis of Table S1 offers profound insights into XLAPn4_9p's molecular dynamics. F column reveals a noteworthy coordination number (at the first minima) obtained from the Radial Distribution Function (RDF) calculated by molecular dynamics simulations. XLAPn4_9p have elevated coordination number of approximately 5, signifying an enhanced propensity for interaction with surrounding water molecules. This elevated coordination suggests a nuanced molecular environment, possibly driven by specific polar interactions or structural features inherent to XLAPn4_9p. Further dissection of the J column illuminates the coordination number (at the first minima) arising from Radial distribution function between tethered charges within the ion exchange membrane and oxygen molecules within the aqueous milieu. XLAPn4_9p showcases a markedly lower coordination number of around 1.5 compared to its counterparts. This discrepancy hints at a distinctive molecular arrangement within the membrane-water interface, possibly influenced by XLAPn4_9p's unique charge distribution or structural characteristics. Moreover, insights gleaned from the N column unveil a coordination number of 0.07 for XLAPn4_9p. This minuscule value underscores the intricacies of molecular

dynamics within XLAPn4_9p, suggesting a delicate balance between tethered charges and ions within the system, which may exert a profound influence on its overall behavior. In essence, the intricate revelations stemming from molecular dynamics simulations not only elucidate the molecular nuances of XLAPn4_9p but also underscore the indispensable role of such simulations in deciphering the intricate intermolecular interactions within polymer-salt systems. These insights hold profound implications for materials design and engineering across diverse applications, ranging from membrane technologies to advanced drug delivery systems, by providing a deeper understanding of structure-property relationships at the molecular level.

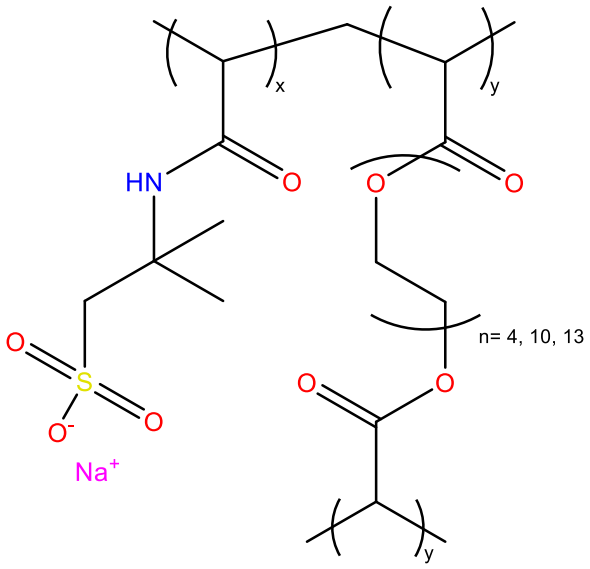

Figure 8: Structure of ionomers with Na^+ counter ion in XLAPn4_9p[56] anion exchange membranes.

Moreover, **Figure 9** illustrates the error distribution across an 11-fold cross-validation for the model (seed number 28 with a batch size of 10, 256 hidden neurons, and a learning rate of 0.005), both with and without MD descriptors, respectively. The distributions of Mean Squared Error (MSE) shed light on the internal consistency of the models' predictive performance. Notably, the model incorporating MD descriptors exhibited lower variation in training MSE, suggesting stability during the training part. However, during the testing part, the MSEs displayed slightly more fluctuation, indicating varied model performance across different validation folds. This

variability emphasizes the challenge of generalizing the model to new data and underscores its sensitivity to the diversity of test samples.

Conversely, the model lacking MD descriptors displays higher variability in both training and testing MSEs, implying reduced consistency and reliability in its predictions. Such significant fluctuation across folds hints at a risk of overfitting, wherein the model memorizes the training data rather than learning to generalize from it. This poses a significant concern in practical applications, where the model's performance on unseen data is crucial. The absence of MD descriptors appears to strip the model of crucial features necessary for a nuanced comprehension of complex data patterns, potentially elucidating its heightened sensitivity to variations in test samples.

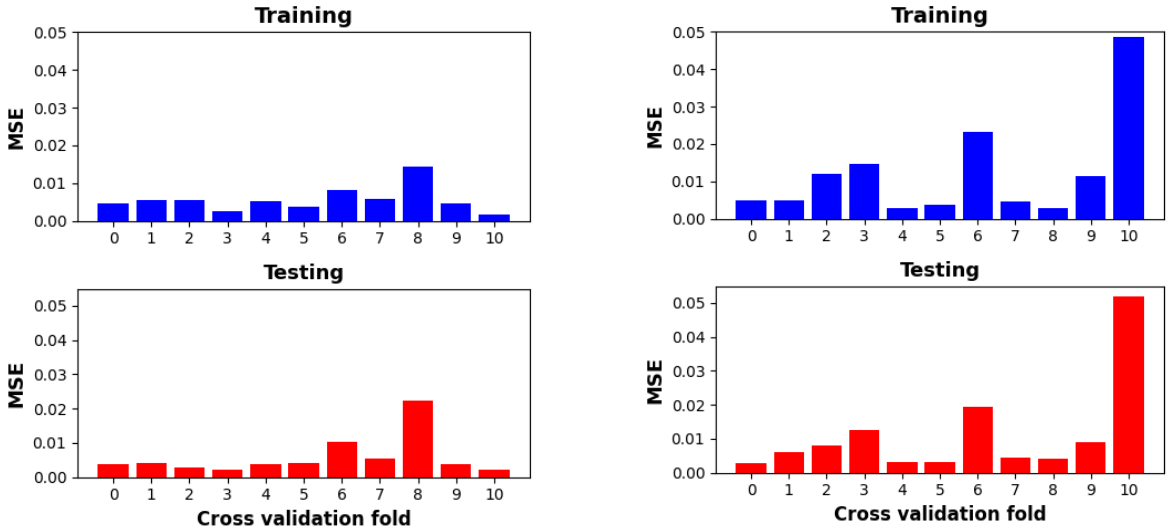

(a) (b)

Figure 9: Error distribution of the trained models for 11 cross validations: (a) with MD Descriptors and (b)without MD descriptors.

In Figure S1, The behavior of the loss function during training of the model (seed number 28 with a epochs of 10, 256 hidden neurons, and a learning rate of 0.005) unveils a significant contrast: while both loss function curves exhibit bumps and irregularities, the curve associated with Molecular Dynamics (MD) descriptors displays a finely tuned trajectory at the end of training by 1000 epochs, in stark contrast to the more fluctuating nature of the curve in their absence.

In a nutshell, the integration of molecular dynamics (MD) descriptors into the Graph Convolutional Network (GCN) model significantly enhances its predictive capabilities and robustness. By incorporating MD descriptors, the GCN model demonstrates a closer alignment between its distribution plot and experimental values of activity coefficients. This convergence between predicted and observed values underscores the model's improved accuracy in capturing the intricate dynamics of molecular interactions. Moreover, the inclusion of MD descriptors empowers the GCN model to exhibit greater resilience against variations in initial conditions, thereby enhancing its overall robustness. This synergistic integration of MD descriptors into the GCN framework not only advances our understanding of molecular behavior but also offers a promising avenue for more accurate predictions in chemical research.

4.3. Saliency Analysis

Ion exchange membranes (IEMs) are mainly consist of charged functional groups covalently attached to the polymer backbone or matrix.[13, 57] These functional groups can ionize in polar solvents such as water. As illustrated in **Figure 10**, cation exchange membranes (CEMs) are membranes with negatively charged (e.g., sulfonate) groups, and anion exchange membranes (AEMs) are with positively charged (e.g., quaternary amines) groups. In an IEM, the fixed anions are in electrical balance with mobile cations (counterions) in the polymer's interstices.[13] In contrast, the mobile anions, also known as co-ions, are largely excluded from the polymer matrix due to having the same electrical charge as fixed ions. Consequently, CEMs only allow the transfer of cations, whereas AEMs only allow the transfer of anions.[57]

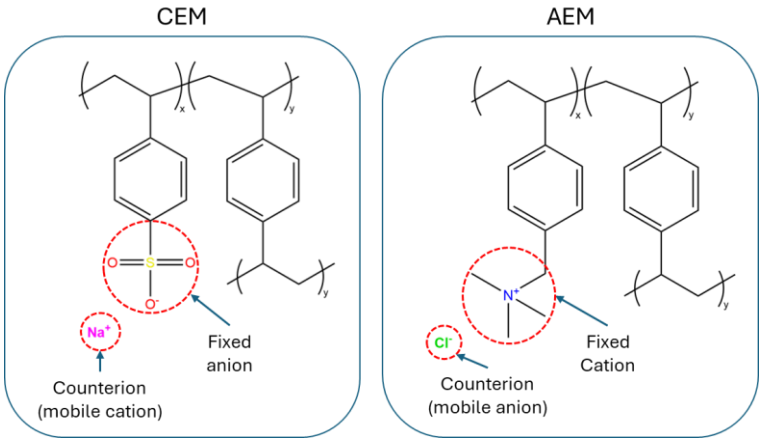

Figure 10: Schematic representation of a Cation-Exchange Membrane (CEM) and an Anion-Exchange Membrane (AEM). The diagram illustrates the fixed charge functional groups and their corresponding counterions within each membrane type. The CEM shows a negatively charged sulfonate group with a sodium (Na^+) counterion, while the AEM displays a positively charged quaternary ammonium group with a chloride (Cl^-) counterion.

To better understand the interactions within these membranes, saliency maps have been employed to interpret the results from Graph Neural Networks (GNNs) trained using SMILES of the polymer IEMs representations to predict the ion activity coefficients. These maps highlight the relative importance of atoms or groups within the molecular structure based on GNN. This method allows for a more detailed interpretation of the complex mechanisms of GNNs by projecting these saliency maps onto the 2D molecular structures, thus making it possible to visually analyze which substructures are crucial for the functionality of the membranes on the predicted activity coefficient. Therefore, our analysis would mainly focus on the interpretation of the fixed charged groups and the counterions in the CEMs and AEMs. **Figure 11** shown the saliency maps computed for nine molecules present in our data set. The atoms (nodes in the graph representation) are colored according to their normalized gradients. Red regions of the molecule indicate positive gradients, signifying that increasing the feature value associated with this part of the molecule would raise the predicted activity coefficient. Conversely, blue regions often denote areas where the gradient is negative, implying that increasing the feature value would lower the predicted activity coefficient.

In cases where the fixed ionomer contains a positive tethered charge (N^+), we generally observe a blue color, indicating a decrease in the predicted activity coefficient, as seen in PSbNP-BCE and PSbNP-RCE among the AEMs (refer to **Figure 11** and **Table 4**). However, an anomaly appears with AR204, where the N^+ displays a red color, suggesting a positive influence on the activity coefficient. This discrepancy, where the predicted value (0.39) significantly exceeds experimental ranges (0.08-0.27), may indicate a prediction error. Furthermore, the presence of aromatic ring systems seems to challenge the model's ability to highlight the relevance of the tethered charges in the saliency maps, possibly due to the aromatic rings altering electron density, which in turn affects the activity coefficient—a notable effect in compounds like AR103 and CR61. Conversely, the tethered charge (SO_3^-) in CEMs consistently shows a red tendency color, indicating a positive gradient, which enhances the predicted activity coefficient. This is likely because the sulfonate groups, being highly charged and hydrophilic, significantly increase water uptake in the polymer IEMs, thus boosting ion mobility within the membrane. Regarding counterions in AEMs, iodide (I-) exhibits a red color, indicating a positive gradient and thus suggesting a higher predicted activity coefficient. This is supported by the data obtained from MD solvation descriptors: coordination number (at first minima) from Radial distribution function between counterion and oxygen of water (F in **Table 4**) and coordination number (at first minima) from Radial distribution function between tethered charge (in ionomer) and counterion (in salt) (N in **Table 4**). Therefore, iodide exhibits a higher coordination number with the tethered charge (N) despite having a lower coordination number with the oxygen in water (F) compared to chloride (Cl-). This implies that iodide's interaction with the tethered charge significantly influences its impact on the activity coefficient. Conversely, chloride, which has a higher interaction with water oxygen (reflected by a higher F value), shows a blue color, indicating a negative gradient and a lower predicted activity coefficient due to its lower coordination number with the tethered charge (N). In CEMs, most counterions are red except for calcium (Ca^{2+}) and potassium (K^+), which are blue. This suggests that Ca^{2+} and K^+interact more with water oxygen than with the ionomer, as evidenced by their higher coordination numbers compared to those of lithium (Li^+), magnesium (Mg^{2+}), and sodium (Na^+). Therefore, the latter set of ions have higher charge density (compared to the much large Ca^{2+} and K^+ ions) and thus interact more strongly with the ionomer charges.

Table 4: Comparative Analysis of Anion-Exchange Membranes (AEMs) and Cation-Exchange Membranes (CEMs) on the saliency analysis. The color representation of the ionomer (fixed charger group) and the counterion from the saliency maps of each polymer. F and N represent the coordination number (at first minima) from Radial distribution function between counterion and oxygen of water and the coordination number (at first minima) from Radial distribution function between tethered charge (in ionomer) and counterion (in salt), respectively.

Type	Polymer	Fixed charge group	Color Fixed charge group	Counterion	Color counterion	F	N	Exp Act Coeff.	Pred Act. Coeff.
AEM	PSbNP-BCE	C_3N^+ (N^+)	lighter blue	I^-	red	4.6-4.7	1.9-2.5	0.16-0.34	0.19
	PSbNP-RCE	C_3N^+ (N^+)	blue			3.94-4.18	1.29-2.44	0.30-0.66	0.21
	AR103	C_3N^+ (N^+)	nothing	Cl^-	lighter blue	7	1.3-1.8	0.11-0.24	0.14
	AR204	C_3N^+ (N^+)	Red		blue	7	1-1.3	0.08-0.27	0.39
CEM	PVAS	SO_3^-	Blue/ Red	Na^+	red	5.29-5.38	0.13-0.25	0.28-0.52	0.19
	CEM	SO_3^-	Blue/ Red			2.5-2.4	0.13-0.3	0.37-0.78	0.44
	XLAMPS	SO_3^-	red			4.04-5.47	0.03-0.31	0.60-1.72	0.67
	Nafion	SO_3^-	red	Na^+	red	4.5-5.2	0.2-0.3	0.13-0.23	0.10
		SO_3^-		Na^+ (SO_4)		2.7-5.1	0.2-0.4	0.001-0.002	0.10
		SO_3^-		Mg^{2+}	lighter red	4.9-5.3	0.12-0.22	0.05-0.36	0.10
	CR61	SO_3^-	lighter red	Na^+	red	4.3-4.6	0.5-0.7	0.13-0.29	0.17
		SO_3^-		Mg^{2+}	lighter red	4.9-5.3	0.12-0.24	0.08-0.41	0.16
		SO_3^-		Li^+	lighter red	2.6-2.7	0.5-0.6	0.11-0.59	0.16
		SO_3^-		Ca^{2+}	lighter blue	5.3-6.1	0.46-0.62	0.05-0.25	0.16
		SO_3^-		K^+	blue	5.4-6	0.5-0.9	0.08-0.27	0.16

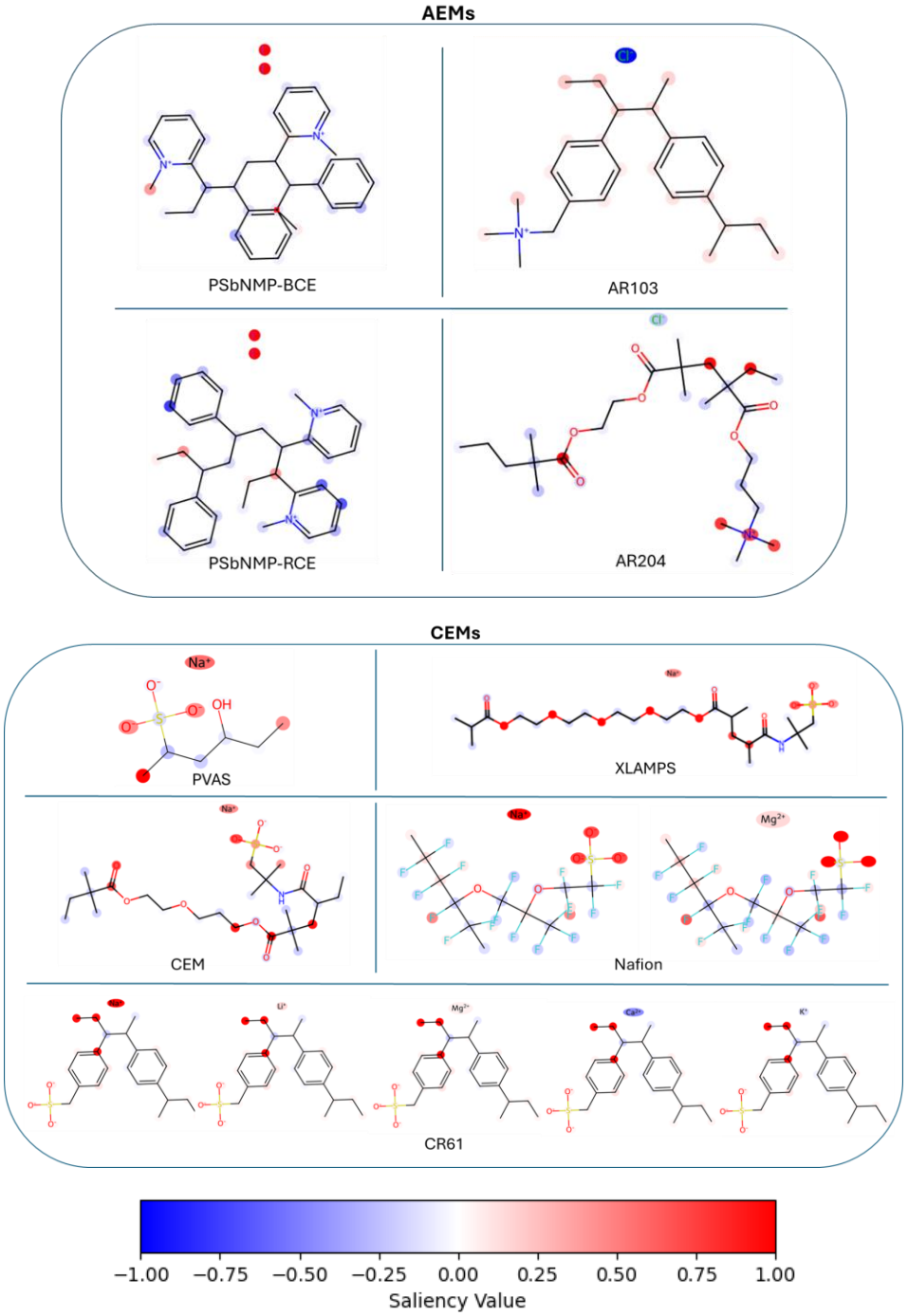

Figure 11: Saliency maps of the molecular structure for various anion-exchange membranes (AEMs) and cation-exchange membranes (CEMs). The top panel displays AEMs, with molecular diagrams for PSbNMP-BCE, AR103, PSbNMP-RCE, and AR204. The bottom panel shows CEMs, including PVAS, XLAMPS, CEM, Nafion, and CR61. Each molecule is color-coded based on the normalized gradients and the color-coded saliency value scale ranging from -1.00 to 1.00: red areas indicate regions where an increase in feature value would raise the predicted activity coefficient, whereas blue areas suggest a decrease.

5. CONCLUSION

In conclusion, our study has successfully shown that the integration of Molecular Dynamics (MD) descriptors into a Graph Convolutional Network (GCN) significantly enhances the model's prediction of activity coefficients. The careful calibration of hyperparameters, particularly the learning rate and the number of hidden neurons, has been shown to be instrumental in optimizing the model's performance.

Through rigorous testing and validation, characterized by 11-fold cross-validation and a variety of performance metrics, we have established that the GCN model with MD descriptors not only better fits to the experimental data, as indicated by higher R^2 values, but also exhibits a more consistent and reliable prediction as reflected by lower standard deviations and Mean Absolute Errors across both training and test sets. Therefore, the findings of the study have important implications for computational chemistry and molecular dynamics, where the need for precise activity coefficient predictions is critical. The enhanced predictive power of the GCN model with MD descriptors could facilitate more accurate simulations of molecular behavior, potentially accelerating the development of new materials and chemicals.

In addition, the saliency maps serve as a powerful exploratory tool in polymer science, offering tangible clues to the molecular features that govern the activity coefficient of IEMs. By harnessing this analytical prowess, researchers can better understand the molecular underpinnings of polymer performance and steer the synthesis of next-generation materials toward optimal functionality.

Furthermore, this research underscores the potential of machine learning models to capture complex physical interactions through appropriate feature engineering and hyperparameter optimization. As we continue to integrate more sophisticated descriptors and refine model architectures, we can expect further advancements in predictive modeling and simulation. Future work will focus on expanding the dataset, exploring additional descriptors, and refining the model architecture to further improve the accuracy and generalizability of the predictions. The promising results obtained here pave the way for the usage advanced machine learning methods to a broader range of challenges in the physical sciences.

Author Information

✓ Corresponding Author

Jose. A. Romagnoli− Cain Department of Chemical Engineering, Louisiana State University, Baton Rouge, Louisiana 70803, United States; orcid.org/0000-0003-3682-1305; Email: jose@lsu.edu

✓ Authors

Pegah Naghshnejad − Cain Department of Chemical Engineering, Louisiana State University, Baton Rouge, Louisiana 70803, United States; orcid.org/0009-0006-8110-8479

Gabriela Theis Marchan − Cain Department of Chemical Engineering, Louisiana State University, Baton Rouge, Louisiana 70803, United States; https://orcid.org/0009-0000-9147-3943

Teslim Olayiwola −Cain Department of Chemical Engineering, Louisiana State University, Baton Rouge, Louisiana 70803, United States; https://orcid.org/0000-0002-7619-5495

Revati Kumar − Department of Chemistry, Louisiana State University, Baton Rouge, Louisiana 70803, United States; orcid.org/0000-0002-3272-8720

ACKNOWLEDGMENT

This work was supported by the U.S Department of Energy, Office of Science, under the Office of Basic Energy Science Separation Science program under Award No. DE-SC0022304. We gratefully acknowledge the computer time allotted by the high-performance computing center (HPC) at LSU and the Louisiana Network initiative.

REFERENCES

(1) Gallage Dona, H. K.; Olayiwola, T.; Briceno-Mena, L. A.; Arges, C. G.; Kumar, R.; Romagnoli, J. A. Determining Ion Activity Coefficients in Ion-Exchange Membranes with Machine Learning and Molecular Dynamics Simulations. *Industrial & Engineering Chemistry Research* **2023**.

(2) Jordan, M. L.; Kulkarni, T.; Senadheera, D. I.; Kumar, R.; Lin, Y. J.; Arges, C. G. Imidazolium-type anion exchange membranes for improved organic acid transport and permselectivity in electrodialysis. *Journal of The Electrochemical Society* **2022**, *169* (4), 043511.
(3) Jordan, M. L.; Kokoszka, G.; Gallage Dona, H. K.; Senadheera, D. I.; Kumar, R.; Lin, Y. J.; Arges, C. G. Integrated Ion-Exchange Membrane Resin Wafer Assemblies for Aromatic Organic Acid Separations Using Electrodeionization. *ACS Sustainable Chemistry & Engineering* **2023**, *11* (3), 945-956.
(4) Feng, Y.; Yang, L.; Liu, J.; Logan, B. E. Electrochemical technologies for wastewater treatment and resource reclamation. *Environmental Science: Water Research & Technology* **2016**, *2* (5), 800-831.
(5) Kim, K.; Baldaguez Medina, P.; Elbert, J.; Kayiwa, E.; Cusick, R. D.; Men, Y.; Su, X. Molecular tuning of redox-copolymers for selective electrochemical remediation. *Advanced Functional Materials* **2020**, *30* (52), 2004635.
(6) Santiago, A. R.; Medina, P. B.; Su, X. Electrochemical remediation of perfluoroalkyl substances from water. *Electrochimica Acta* **2022**, *403*, 139635.
(7) Alkhadra, M. A.; Jordan, M. L.; Tian, H.; Arges, C. G.; Bazant, M. Z. Selective and chemical-free removal of toxic heavy metal cations from water using shock ion extraction. *Environmental Science & Technology* **2022**, *56* (19), 14091-14098.
(8) Tang, C.; Bruening, M. L. Ion separations with membranes. *Journal of Polymer Science* **2020**, *58* (20), 2831-2856.
(9) Palakkal, V. M.; Rubio, J. E.; Lin, Y. J.; Arges, C. G. Low-resistant ion-exchange membranes for energy efficient membrane capacitive deionization. *ACS Sustainable Chemistry & Engineering* **2018**, *6* (11), 13778-13786.
(10) Strathmann, H.; Grabowski, A.; Eigenberger, G. Ion-exchange membranes in the chemical process industry. *Industrial & Engineering Chemistry Research* **2013**, *52* (31), 10364-10379.
(11) Li, N.; Guiver, M. D. Ion transport by nanochannels in ion-containing aromatic copolymers. *Macromolecules* **2014**, *47* (7), 2175-2198.
(12) Sata, T. *Ion exchange membranes: preparation, characterization, modification and application*; Royal Society of chemistry, **2007**.
(13) Kamcev, J.; Paul, D. R.; Freeman, B. D. Ion activity coefficients in ion exchange polymers: applicability of Manning's counterion condensation theory. *Macromolecules* **2015**, *48* (21), 8011-8024.
(14) Al-Sakaji, B. A.; Husseini, G. A.; Darwish, N. A. Impact of Ionic Strength and Charge Density on Donnan Potential in the NaCl-Cation Exchange Membrane System. *Water* **2023**, *15* (21), 3830.
(15) Gregor, H. P.; Gottlieb, M. H. Studies on ion exchange resins. VIII. Activity coefficients of diffusible ions in various cation-exchange resins. *Journal of the American Chemical Society* **1953**, *75* (14), 3539-3543.
(16) Pobelov, I. Thermodynamics of ions in solutions. In *Encyclopedia of Interfacial Chemistry: Surface Science and Electrochemistry*, 2018; pp 299-315.
(17) Briceno-Mena, L. A.; Venugopalan, G.; Arges, C. C.; Romagnoli, J. A. A Machine Learning Approach for Device Design from Materials and Operation Data. In *Computer Aided Chemical Engineering*, Vol. 50; Elsevier, **2021**; pp 279-285.
(18) Qin, S.; Jiang, S.; Li, J.; Balaprakash, P.; Van Lehn, R. C.; Zavala, V. M. Capturing molecular interactions in graph neural networks: a case study in multi-component phase equilibrium. *Digital Discovery* **2023**, *2* (1), 138-151.

(19) Gilmer, J.; Schoenholz, S. S.; Riley, P. F.; Vinyals, O.; Dahl, G. E. Neural message passing for quantum chemistry. In *International conference on machine learning*, **2017**; PMLR: pp 1263-1272.
(20) Duvenaud, D. K.; Maclaurin, D.; Iparraguirre, J.; Bombarell, R.; Hirzel, T.; Aspuru-Guzik, A.; Adams, R. P. Convolutional networks on graphs for learning molecular fingerprints. *Advances in neural information processing systems* **2015**, *28*.
(21) Li, Y.; Li, P.; Yang, X.; Hsieh, C.-Y.; Zhang, S.; Wang, X.; Lu, R.; Liu, H.; Yao, X. Introducing block design in graph neural networks for molecular properties prediction. *Chemical Engineering Journal* **2021**, *414*, 128817.
(22) Back, S.; Yoon, J.; Tian, N.; Zhong, W.; Tran, K.; Ulissi, Z. W. Convolutional neural network of atomic surface structures to predict binding energies for high-throughput screening of catalysts. *The journal of physical chemistry letters* **2019**, *10* (15), 4401-4408.
(23) Arbabzadah, F.; Chmiela, S.; Tkatchenko, A. Quantum-chemical insights from deep tensor neural networks. *Bulletin of the American Physical Society* **2017**, *62*.
(24) Coley, C. W.; Barzilay, R.; Green, W. H.; Jaakkola, T. S.; Jensen, K. F. Convolutional embedding of attributed molecular graphs for physical property prediction. *Journal of chemical information and modeling* **2017**, *57* (8), 1757-1772.
(25) Schweidtmann, A. M.; Rittig, J. G.; Weber, J. M.; Grohe, M.; Dahmen, M.; Leonhard, K.; Mitsos, A. Physical pooling functions in graph neural networks for molecular property prediction. *Computers & Chemical Engineering* **2023**, *172*, 108202.
(26) Chen, C.; Ye, W.; Zuo, Y.; Zheng, C.; Ong, S. P. Graph networks as a universal machine learning framework for molecules and crystals. *Chemistry of Materials* **2019**, *31* (9), 3564-3572.
(27) Aoki, Y.; Wu, S.; Tsurimoto, T.; Hayashi, Y.; Minami, S.; Tadamichi, O.; Shiratori, K.; Yoshida, R. Multitask Machine Learning to Predict Polymer–Solvent Miscibility Using Flory–Huggins Interaction Parameters. *Macromolecules* **2023**, *56* (14), 5446-5456.
(28) Qin, S.; Jin, T.; Van Lehn, R. C.; Zavala, V. M. Predicting critical micelle concentrations for surfactants using graph convolutional neural networks. *The Journal of Physical Chemistry B* **2021**, *125* (37), 10610-10620.
(29) Kensert, A.; Bouwmeester, R.; Efthymiadis, K.; Van Broeck, P.; Desmet, G.; Cabooter, D. Graph convolutional networks for improved prediction and interpretability of chromatographic retention data. *Analytical Chemistry* **2021**, *93* (47), 15633-15641.
(30) Paszke, A.; Gross, S.; Massa, F.; Lerer, A.; Bradbury, J.; Chanan, G.; Killeen, T.; Lin, Z.; Gimelshein, N.; Antiga, L. Pytorch: An imperative style, high-performance deep learning library. *Advances in neural information processing systems* **2019**, *32*.
(31) Deng, D.; Chen, X.; Zhang, R.; Lei, Z.; Wang, X.; Zhou, F. XGraphBoost: extracting graph neural network-based features for a better prediction of molecular properties. *Journal of chemical information and modeling* **2021**, *61* (6), 2697-2705.
(32) Zhang, S.; Tong, H.; Xu, J.; Maciejewski, R. Graph convolutional networks: a comprehensive review. *Computational Social Networks* **2019**, *6* (1), 1-23.
(33) Zhang, Y.; Jiang, Q.; Xu, M.; Zhang, Y.; Liu, J.; Jia, P. FTM-GCN: A novel technique for gas concentration predicting in space with sensor nodes. *Sensors and Actuators B: Chemical* **2024**, *399*, 134830.
(34) Landrum, G. RDKit: Open-source cheminformatics. 2006. *Google Scholar* **2006**.
(35) Javaloy, A.; Sanchez-Martin, P.; Levi, A.; Valera, I. Learnable graph convolutional attention networks. *arXiv preprint arXiv:2211.11853* **2022**.

(36) Heid, E.; Greenman, K. P.; Chung, Y.; Li, S.-C.; Graff, D. E.; Vermeire, F. H.; Wu, H.; Green, W. H.; McGill, C. J. Chemprop: A machine learning package for chemical property prediction. *Journal of Chemical Information and Modeling* **2023**, *64* (1), 9-17.
(37) Kipf, T. N.; Welling, M. Semi-supervised classification with graph convolutional networks. *arXiv preprint arXiv:1609.02907* **2016**.
(38) Ramos-Garcés, M. V.; Li, K.; Lei, Q.; Bhattacharya, D.; Kole, S.; Zhang, Q.; Strzalka, J.; Angelopoulou, P. P.; Sakellariou, G.; Kumar, R. Understanding the ionic activity and conductivity value differences between random copolymer electrolytes and block copolymer electrolytes of the same chemistry. *RSC advances* **2021**, *11* (25), 15078-15084.
(39) Lei, Q.; Li, K.; Bhattacharya, D.; Xiao, J.; Kole, S.; Zhang, Q.; Strzalka, J.; Lawrence, J.; Kumar, R.; Arges, C. G. Counterion condensation or lack of solvation? Understanding the activity of ions in thin film block copolymer electrolytes. *Journal of materials chemistry A* **2020**, *8* (31), 15962-15975.
(40) Thompson, A. P.; Aktulga, H. M.; Berger, R.; Bolintineanu, D. S.; Brown, W. M.; Crozier, P. S.; In't Veld, P. J.; Kohlmeyer, A.; Moore, S. G.; Nguyen, T. D. LAMMPS-a flexible simulation tool for particle-based materials modeling at the atomic, meso, and continuum scales. *Computer Physics Communications* **2022**, *271*, 108171.
(41) Jorgensen, W. L.; Maxwell, D. S.; Tirado-Rives, J. Development and testing of the OPLS all-atom force field on conformational energetics and properties of organic liquids. *Journal of the American Chemical Society* **1996**, *118* (45), 11225-11236.
(42) Jorgensen, W. L.; Tirado-Rives, J. The OPLS [optimized potentials for liquid simulations] potential functions for proteins, energy minimizations for crystals of cyclic peptides and crambin. *Journal of the American Chemical Society* **1988**, *110* (6), 1657-1666.
(43) Wang, J.; Wolf, R. M.; Caldwell, J. W.; Kollman, P. A.; Case, D. A. Development and testing of a general amber force field. *Journal of computational chemistry* **2004**, *25* (9), 1157-1174.
(44) Jorgensen, W. L.; Chandrasekhar, J.; Madura, J. D.; Impey, R. W.; Klein, M. L. Comparison of simple potential functions for simulating liquid water. *The Journal of chemical physics* **1983**, *79* (2), 926-935.
(45) Frisch, M. J.; Trucks, G.; Schlegel, H.; Scuseria, G.; Robb, M.; Cheeseman, J.; Scalmani, G.; Barone, V.; Mennucci, B.; Petersson, G. Gaussian 09, rev. *Gaussian Inc, Wallingford* **2009**.
(46) Wang, J.; Wang, W.; Kollman, P. A.; Case, D. A. Automatic atom type and bond type perception in molecular mechanical calculations. *Journal of molecular graphics and modelling* **2006**, *25* (2), 247-260.
(47) Moreno, G. R.; Niranjan, M.; Prugel-Bennett, A. Saliency map on CNNS for protein secondary structure prediction. In *ICASSP 2019-2019 IEEE International Conference on Acoustics, Speech and Signal Processing (ICASSP)*, 2019; IEEE: pp 1249-1253.
(48) Akita, H.; Nakago, K.; Komatsu, T.; Sugawara, Y.; Maeda, S.-i.; Baba, Y.; Kashima, H. Bayesgrad: Explaining predictions of graph convolutional networks. In *Neural Information Processing: 25th International Conference, ICONIP 2018, Siem Reap, Cambodia, December 13–16, 2018, Proceedings, Part V 25*, 2018; Springer: pp 81-92.
(49) Hu, J.; Li, Z.; Lin, J.; Zhang, L. Prediction and Interpretability of Glass Transition Temperature of Homopolymers by Data-Augmented Graph Convolutional Neural Networks. *ACS Applied Materials & Interfaces* **2023**, *15* (46), 54006-54017.
(50) Adebayo, J. a. G. J. a. M. M. a. G. I. a. H. M. a. K. B. Sanity Checks for Saliency Maps. In **2018**.

(51) Tokui, S.; Oono, K.; Hido, S. Chainer: a next-generation open source framework for deep learning.
(52) Galizia, M.; Benedetti, F. M.; Paul, D. R.; Freeman, B. D. Monovalent and divalent ion sorption in a cation exchange membrane based on cross-linked poly (p-styrene sulfonate-co-divinylbenzene). *Journal of membrane science* **2017**, *535*, 132-142.
(53) Sujanani, R.; Katz, L. E.; Paul, D. R.; Freeman, B. D. Aqueous ion partitioning in Nafion: Applicability of Manning's counter-ion condensation theory. *Journal of Membrane Science* **2021**, *638*, 119687.
(54) Nagasawa, M.; Izumi, M.; Kagawa, I. Colligative properties of polyelectrolyte solutions. V. Activity coefficients of counter-and by-ions. *Journal of Polymer Science* **1959**, *37* (132), 375-383.
(55) Jang, E.-S.; Kamcev, J.; Kobayashi, K.; Yan, N.; Sujanani, R.; Talley, S. J.; Moore, R. B.; Paul, D. R.; Freeman, B. D. Effect of water content on sodium chloride sorption in cross-linked cation exchange membranes. *Macromolecules* **2019**, *52* (6), 2569-2579.
(56) Yan, N.; Sujanani, R.; Kamcev, J.; Galizia, M.; Jang, E.-S.; Paul, D. R.; Freeman, B. D. Influence of fixed charge concentration and water uptake on ion sorption in AMPS/PEGDA membranes. *Journal of Membrane Science* **2022**, *644*, 120171.
(57) Strathmann, H. *Ion-exchange membrane separation processes*; Elsevier, 2004.